Waveguide electro-optic modulators based on intrinsically polar self-assembled superlattices (SASs)

Zhifu Liu[a*], Seng Tiong Ho [a], Seongsik Chang [a], Yiguang Zhao [a],
Tobin J. Marks [b], Hu Kang [b], Milko E. van der Boom[b], and Peiwang Zhu [b]

[a] Department of Electrical and Computer Engineering,
Northwestern University, Evanston, IL 60208

[b] Department of Chemistry and Materials Research Center,
Northwestern University, Evanston, IL 60208

ABSTRACT

In this paper we describe methods of fabricating and characterizing organic electro-optic modulators based on intrinsically polar self-assembled superlattices. These structures are intrinsically acentric, and exhibit large second harmonic generation and electro-optic responses without the requirement of poling by an external electric field. A novel wet chemical protection-deprotection approach for the growth of self-assembled superlattices has been developed, and the refractive indices of self-assembled organic electro-optic superlattices may be tuned during the self-assembly process. Prototype electro-optic modulators based on chromophoric self-assembled superlattices have been designed and fabricated. The effective electro-optic coefficient of the self-assembled superlattice film in a phase modulator is estimated as about 20 pm/V at a wavelength of 1064 nm.

Keywords: Polymer thin films, electro-optic materials, self-assembled superlattices, electro-optic modulators

1. INTRODUCTION

Organic materials have attracted remarkable interest recently as promising candidates for fast electro-optic (EO) modulators with low driving voltage.[1,2] For organic crystals, large EO coefficients have been demonstrated for 2-methyl-4-nitroaniline (m-NA)[3], N-(4-nitrophenyl)-(L)-prolinol (NPP)[4], and 4-N,N-dimethylamino-4'-methyl-stilbazolium tosylate (DAST).[5] Research groups also have reported the fabrication of polymer-based EO modulators.[6, 7] The nonlinearity of the polymeric materials was achieved by an external electric field poling process. High modulation rates (110 GHz) were demonstrated.[8] The poled polymer films have two independent electro-optic coefficients. Several methods have been proposed for the measurement of the electro-optic coefficients of polymeric materials.[9,10] An EO polymer device design that eliminated the relaxation of the chromophore alignment has also been proposed.[11] Another potential approach for fabricating nonlinear waveguides is based on the Langmuir-Blodgett (LB) deposition technique. Second harmonic generation (SHG) from an LB waveguide overlay, coated on a side-polished single-mode optical fiber, has been reported.[12] The common configurations of polymer modulators include the birefringence modulator, the Mach-Zehnder modulator, and the directional coupler.[13]

We describe here an approach to fabricating and characterizing organic EO modulators using multilayer self-assembled superlattices (SAS) as the guiding layer and commercial low-loss polymers as the cladding layers. The SAS layers are acentric and have relatively large EO responses without the requirement of external electric field poling of the materials. The waveguide EO modulators were fabricated by using E-beam, plasma enhanced chemical vapor deposition (PECVD), spin coating, photolithography and reactive ion etching (RIE) process.

* Correspondence: Email: zhifuliu@excite.com; telephone: 847 467 2169

2. Self-Assembled Superlattice (SAS) Materials

Chromophore synthesis

One important step in the fabrication of the organic EO modulators is the growth of multilayer SAS materials on pretreated semiconductor Si or GaAs substrates. The pretreatment includes the deposition of gold electrode and the cladding layers. Previously, SiO_2 (about 2 μm deposited by PECVD) functioned as the cladding layer on which the multilayer SAS will be grown.[14,15] The chromophore synthesis process is shown in Fig. 1. Reaction of the chromophore precursor 4-[[4-[*N*,*N*-bis((*tert*-butyldimethylsiloxy)ethyl)-amino]phenyl]azo]pyridine with

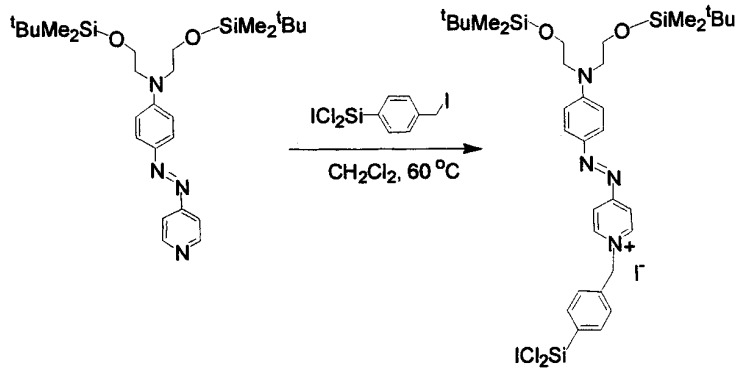

Fig. 1. Chromophore synthesis process.

dichloroiodo[(4-iodomethyl)phenyl]silane in dry CH_2Cl_2 results in quantitative formation of the 4-[[4-[*N*,*N*-bis((*tert*-butyldimethylsiloxy)ethyl)amino]phenyl]azo]dichloroiodo[(4-methyl)phenyl]silane-pyridinium iodide salt. More details have been reported elsewhere.[16]

The growth of self-assembled superlattices

Recently, SAS multilayers have been successfully grown on O_2 treated thin film layers of the high transparency polymer polybisbenzocyclobutane (BCB). An expeditious siloxane-based layer-by-layer assembly process for the growth of intrinsically polar organic EO SAS thin films has been realized.[17] This all-"wet-chemical" two-step procedure has been efficiently implemented in a vertical dipping process to yield SAS films consisting of alternating chromophore and capping layers (Fig. 2). It involves iterative combination of self-limiting polar chemisorption of $-SiCl_2I$-functionalized, high-β chromophore monolayers, and *in situ* protecting group removal followed by self-limiting capping layer formation. The *t*-butyldimethylsiloxy (TBDMS) protecting group in the chromophore can be easily removed (step ii, Fig. 2) by capping agent octachlorotrisiloxane. The nanoscale bilayers (about 3.26 nm thick for each chromophore

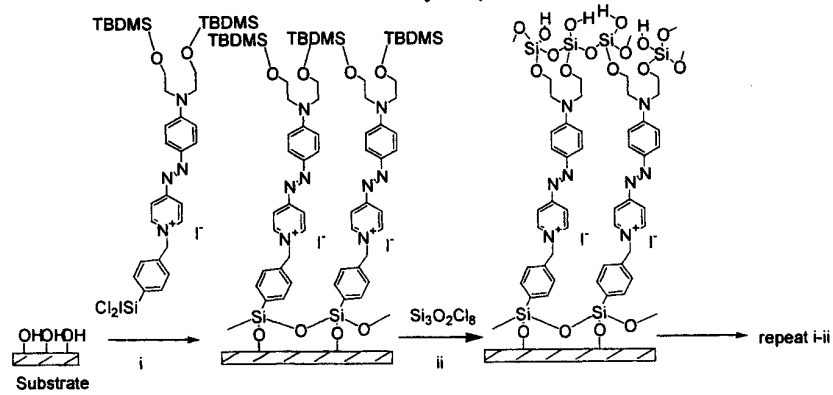

Fig. 2. Schematic of the two-step layer-by-layer self-assembly of self-assembled superlattices.

and polysiloxane bilayer) can be grown at a rate of about 40 min. per bilayer, and it is at least one order of magnitude more rapid than conventional siloxane-based solution deposition methodologies. The chromophore monolayer deposition from solution reaches completion in about 15 min. at 55 °C. The adherent, structurally regular assemblies exhibit appreciable nonlinear responses ($\chi^{(2)}$ ~180 pm/V at a wavelength of 1064 nm) and high chromophore surface densities (about 2.5×10^{14}chromophores/cm^2). Fig. 3 shows the regularity of the SAS layers. The SAS samples have

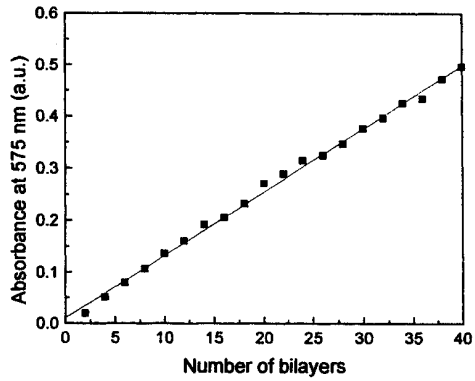

Fig. 3. Optical absorption spectra of SAS films at 575 nm as a function of the number of chromophore-based bilayers. The solid line is the fit by linear regression.

been characterized by various physicochemical techniques, including optical spectroscopy, aqueous contact-angle measurements, specular x-ray reflectivity, atomic force microscopy, and angle-dependent polarized second harmonic generation.

Refractive index tuning of SAS structures

In order to obtain high figures-of-merit of EO modulators, the refractive indices of self-assembled organic EO superlattices may be tuned by intercalating high-Z optically transparent group 13 metal oxide sheets into the structures during the self-assembly process. Microscopic scale regular acentricity and relatively large EO responses are retained in this synthetic procedure.[18] Fig. 4 demonstrates the extent to which the SAS index of refraction can be tuned.

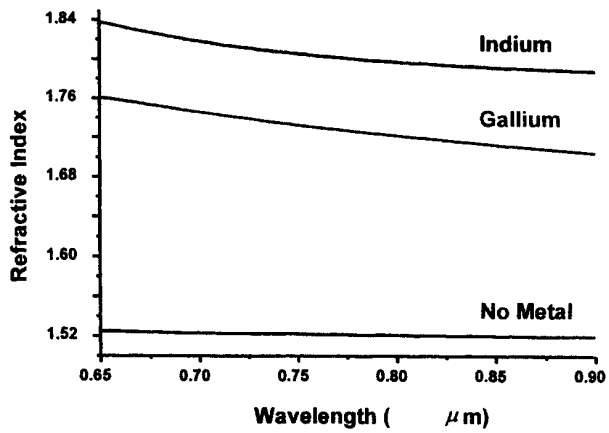

Fig. 4. Refractive index data for metal oxide intercalated SAS films.

3. EO Modulator Device Design and Fabrication

Discussion of polymer rib waveguides

The cross-section of a typical rib waveguide is shown in Fig. 5. The bottom electrode is under the lower cladding layer,

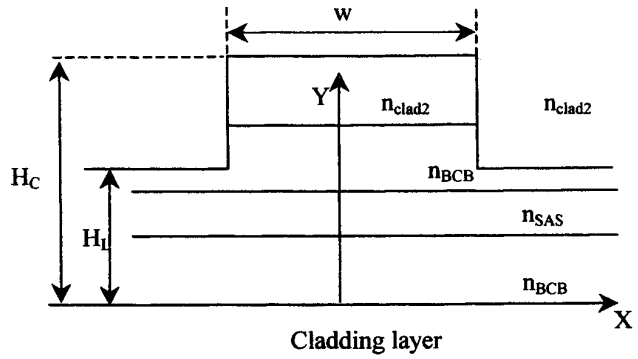

Fig. 5. Cross-section of a rib waveguide. Y denotes the vertical direction of the rib waveguide.

and the top electrode is above the top cladding layer. The optical modes propagating in the waveguide may be calculated by the beam propagation method (BPM). As a good estimation, in order to find the single mode condition for the rib waveguide, the rib waveguide is divided into one central region and two lateral regions. The width of the central region is w, and the height of this region is H_C. The height of the lateral regions is H_L. For each of the three regions, we used an approach that treated the region as a multilayer planar waveguide and applied transfer matrices that connected adjacent layers.[19] Effective TE (or TM) mode refractive indices may be obtained for each region. The resultant effective indices for the three regions are used as TM (or TE) refractive index parameters of a symmetric three layer waveguide with guiding layer thickness w.[20] The original central region of the rib waveguide may accommodate higher order traveling modes as well as the fundamental mode. If the lowest mode refractive index of the lateral region is larger than that of the first order mode in the central region, the whole rib waveguide may be remain single mode one because the energy of the higher order modes in the central region will couple into the lateral regions and dissipate quickly. The rib waveguide structure allows a large cross-section for single traveling mode waveguides, which makes possible a good match of the optical mode with the core section of an optical fiber. Due to the small difference of the effective refractive indices between the central and the lateral regions and the changeable rib waveguide width w, it is usually possible to fabricate a large cross-section waveguide in which only the fundamental mode remains traveling after a relatively long distance (at the millimeter level).

The EO modulator fabrication

The electro-optic waveguide modulator configuration is shown schematically in Fig. 6 and has a five-layer stack structure fabricated by photolithography and RIE processes. The polymer CYTOP (Fig. 7a, from Asahi Glass Co. , C/O

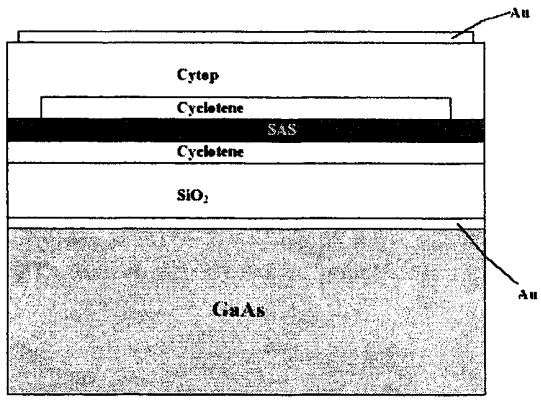

Fig. 6. Schematic cross-section of the traveling wave EO modulator.

Bellex International Corp., Wilmington, DE 19809) is used for the upper cladding layer, while SiO_2 functions as the lower cladding layer. In the waveguide structure, SAS combined with layers of the polymer BCB (Fig. 7b, from Dow Chemical Co., Midland, MI 48674) serve as the guiding layer.

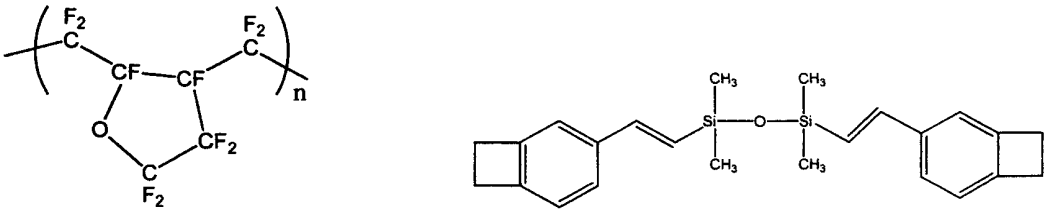

(a) (b)

Fig. 7. Structures of polymers (a) CYTOP, and (b) BCB (Cyclotene 3022-35).

The refractive index of BCB (n = 1.56 at a wavelength of 1064 nm) is very close to that of the SAS, and the refractive index of CYTOP is 1.34 at a wavelength of 1064 nm. Both CYTOP and BCB exhibit good transparency over a wide wavelength range from the ultraviolet to infrared. Gold (500 nm thick) was deposited on Si or GaAs substrate by E-beam method. To make the bonding between gold and the substrate more robust, a narrow layer of Ti (about 30 nm) was fabricated first on the substrate. A cladding layer of SiO_2 (about 2 microns) was then evaporated on the metal electrode by PECVD process. One layer of polymer BCB was spin coated on the silicon dioxide. The thickness of the layer was measured by a prism coupler, optical profiler, or SEM device.

The self-assembled superlattice multilayers were grown on the reactive ion etching treated BCB layer. The RIE treatment of the surface of BCB using O_2 gas ensures that there are ample silanol groups present for SAS growth on the treated BCB surface. The thickness of 100 SAS layers is about 0.34 μm. A second layer of BCB was then spin coated on the surface of the SAS layers. In order to reduce the loss due to the electrodes of the final waveguide, the thickness of both the BCB layers were chosen to be in the order of 1 μm. The BCB has a closely matched refractive index with the SAS materials for a relatively broad wavelength range. The BCB/SAS/BCB triple layer structure functions as the guiding layer of the waveguide. A cladding layer of polymer CYTOP CTX-809A was then spin coated on the top BCB layer. Contact printing lithography (apply AZ series positive photoresist on the sample, soft bake for about 60 seconds on a hot plate, expose and develop) and RIE (using a mixture of O_2, Ar, and CF_4 gases) processes were used to develop rib waveguide patterns on the polymer multi-layer structure. Analysis and simulation have shown that for given

waveguide width (6.0 μm for one sample), a proper etching depth of the polymer layers may be chosen so as to allow the rib waveguide accommodate only a single optical mode. Then another layer of CYTOP, functioning as a cladding layer, was spin coated onto the first CYTOP layer. The top Au electrode (30 μm wide, and 0.4 μm in thickness) was fabricated using negative photoresist and lift-off techniques.

The match between the optical and RF waves

The RF bandwidth is related to the velocity mismatch between the optical and RF waves and the RF electrode loss. For low loss materials, the parameters $n_{eff\text{-}opt}$ (the effective optical wave refractive index) and $n_{eff\text{-}rf}$ (the effective RF wave refractive index) are needed for the evaluation of the RF bandwidth. The frequency response of the electro-optic modulator is given by

$$H(f) = \frac{\sinh(\frac{\xi L}{2})}{\left(\frac{\xi L}{2}\right)}, \tag{1}$$

where $\xi = 2\pi f(n_{eff\text{-}opt} - n_{eff\text{-}rf})/c$ and f is the frequency. We have assumed that the electrode loss α is negligible here. The RF bandwidth, f_{3dB} , is given by $H(f_{3dB}) = 1/\sqrt{2}$. The index $n_{eff\text{-}opt}$ was estimated using a rib waveguide configuration as discussed in the previous section (Fig. 8).

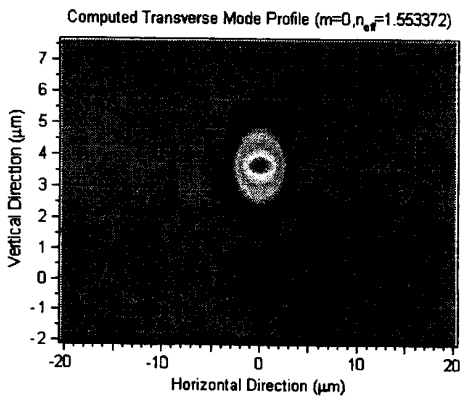

Fig. 8. One of the typical optical modes traveling within the rib waveguide.

The index $n_{eff\text{-}rf}$ is given by

$$n_{eff-rf} = \sqrt{\frac{C}{C_0}}, \tag{2}$$

where C is the capacitance with the materials presented and C_0 is that without materials (replaced by air) for a unit length segment of the waveguide. The capacitance calculation was then carried out using finite element analysis methods. The characteristic impedance Z is linked with the capacitances by

$$Z = \frac{1}{c\sqrt{CC_0}}, \tag{3}$$

where c is the speed of light in vacuum. Fig. 9 is one of the typical simulation results of the external electric field distribution in the rib waveguide.

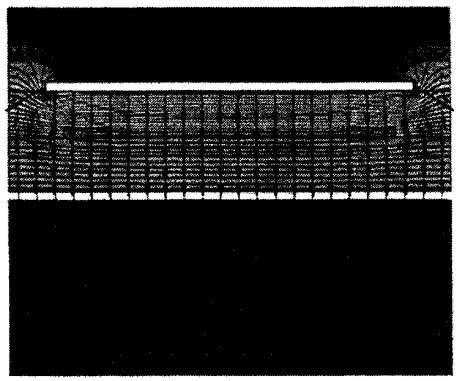

Fig. 9. The simulation result of the external electric field distribution in the microstrip waveguide structure.

In one of the simulation samples, the effective optic refractive index $n_{eff\text{-}opt}$ is found to be 1.556 at a wavelength of 1.064 μm. The capacitance of the sample C is 106 pF. When the materials are replaced by air, the capacitance C_0 of the virtual sample is 37.8 pF, and the effective RF refractive index $n_{eff\text{-}rf}$ is 1.675. The characteristic impedance Z is 52.7 Ω, which is quite close to the 50 Ω ideal value. The difference between the $n_{eff\text{-}opt}$ and $n_{eff\text{-}rf}$ is about 0.119, and this ensures that one can achieve a bandwidth of 40 GHz for a waveguide EO modulator based on the SAS materials and the rib structure.

4. EXPERIMENTAL RESULTS AND DISCUSSION

The thickness of cladding layers and the guiding layers and the RIE-derived rib waveguide depth were estimated by using prism coupler, optical profiler, and SEM instrumentation. Fig. 10 shows one typical result for the BCB polymer

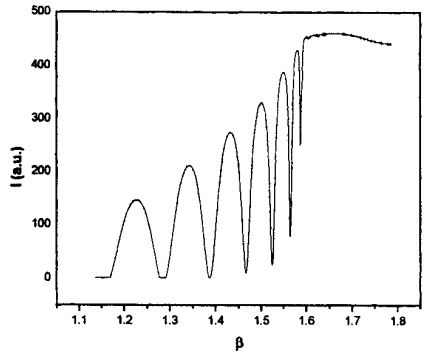

Fig. 10. The TE modes of a BCB polymer layer. Parameter I is the reflected intensity in a.u.

layer (with thickness ~ 2 μm, refractive index ~ 1.55 at a wavelength of 633 nm). Fig. 11 shows the absorption spectra of BCB and CYTOP in UV-VIS region. BCB and CYTOP thin films were made by spin coating the materials on microscopic slides.

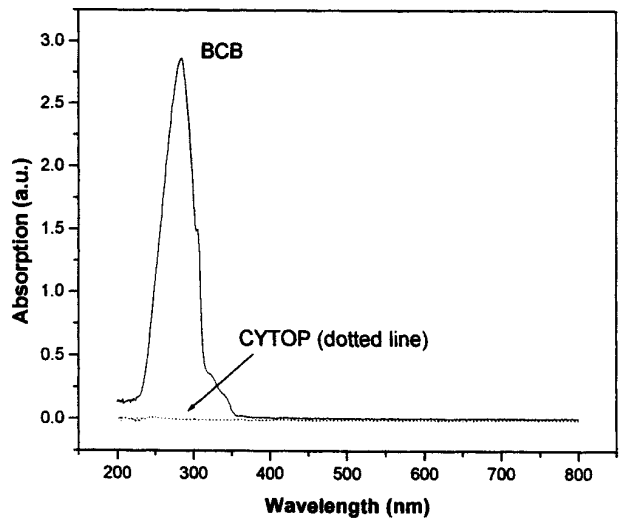

Fig. 11. UV-VIS absorption spectra of BCB and CYTOP samples. BCB and CYTOP thin films were spin coated on microscopic slides.

The refractive index of an SAS film versus wavelength is presented in Fig. 12.

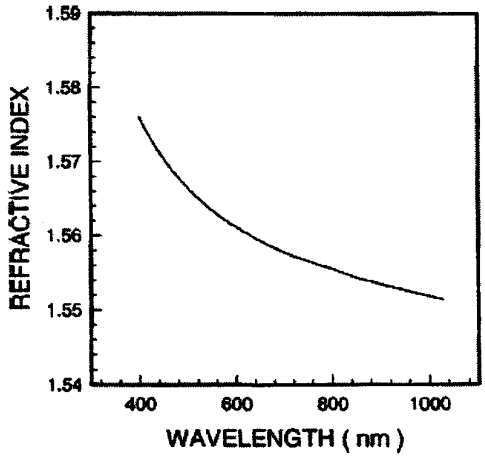

Fig. 12. Wavelength dependence of the refractive index of a self-assembled superlattice film.

Fig. 13 shows two SEM images of the surface profile of the rib waveguide before the upper cladding layer of CYTOP was applied by spin coating (a), and the upper electrode pattern (b).

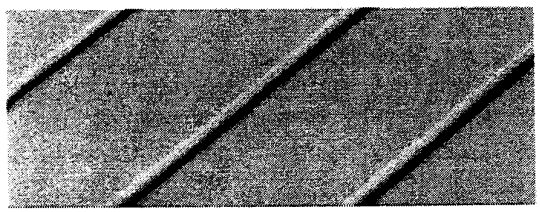

(a)

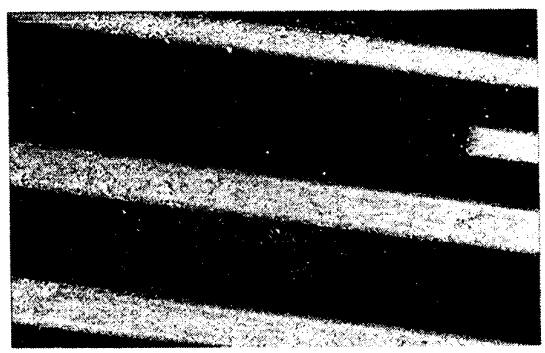

(b)

Fig. 13. SEM images of (a) the rib waveguide, and (b) the upper electrodes.

Driving voltage measurements on the EO modulator

The EO response of the SAS-based waveguide EO modulator was measured by end firing 1064 nm light from a diode pumped Nd:YAG laser, and the light was coupled into and out of the rib waveguide using a pair of 40× microscope objectives. The light beam propagates through a polarizer oriented at 45° with respect to the vertical direction before the objectives. The device was operated by launching both transverse electric and transverse magnetic modes into the waveguide. Then the light goes through an analyzer oriented perpendicular to orientation of the polarizer. The modulated light signal was then coupled to a photodetector, and was monitored by an oscilloscope. Figure 14 shows the typical EO response of the modulator measured from the oscilloscope traces. Trace 1 and trace 2 in Fig. 14 represent the

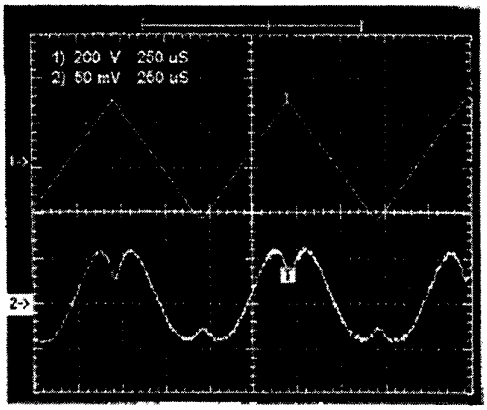

Fig. 14. EO response from a prototype EO modulator based on the SAS. Trace 1 is the applied electrical signal, and trace 2 is the response of the EO modulator.

applied electrical signal and the response signal of the modulator, respectively. The half-wave voltage V_π is estimated to be about 340 V for a 5 mm long waveguide. The half-wave voltage V_π is related to the effective EO coefficient by

$$V_\pi = \frac{\lambda d}{n_{eff-opt}^{3} r L \Gamma}, \tag{4}$$

where λ is the wavelength of the optical wave, d the distance between the lower and the upper electrodes, r the effective EO coefficient, L the length of the electro-optic interaction region, and Γ the overlap of the optical profile and the external electric field. The effective EO coefficient is thus estimated to be about 20 pm/V, in good agreement with that estimated from SHG data. A longer waveguide (at the cm lever) and thicker layers (at the μm level, parameter Γ also will be improved to around 0.8) of the EO-active self-assembled superlattices will help in achieving a much lower V_π.

5. CONCLUSIONS

Organic materials are promising candidates for fast EO modulators for use in future high bandwidth optical fiber communications (OFC). In this paper we described methods of fabricating and characterizing novel organic EO materials composed of self-assembled superlattices (SASs). These structures are intrinsically acentric and exhibit large second harmonic generation (SHG) and EO responses without the necessity of poling with an external electric field. This approach using SAS electro-optic materials has advantages such as no requirement of poling for creating nonlinearity in the films and easy film growth over a large area.

Prototype waveguide EO modulators have been fabricated using SAS films sandwiched between low-loss polymeric guiding and cladding layers of appropriate refractive indices. The waveguide EO modulators were fabricated using a multistep process including E-beam, plasma enhanced chemical vapor deposition (PECVD), spin coating, photolithography and reactive ion etching (RIE) techniques. The velocity mismatch between the optical and RF waves, the RF bandwidth, and EO modulator parameters such as the half-wave voltage and the effective EO coefficient have been evaluated.

6. ACKNOWLEDGMENTS

This work was supported by DARPA/ARO (DAAD 19-00-1-0368), and by the MRSEC program of the National Science Foundation (DMR-0076097) at Northwestern University.

7. REFERENCES

1. Y. Q. Shi, C. Zhang, H. Zhang, J. H. Bechtel, L. R. Dalton, B. H. Robinson, and W. H. Steier, "Low (sub-1-volt) halfwave voltage polymeric electro-optic modulators achieved by controlling chromophore shape", *Science* **288**, 119-122 (2000).
2. S. R. Marder, B. Kippelen, A. K. Y. Jen, and N. Peyghambarian, "Design and synthesis of chromophores and polymers for electro- optic and photorefractive applications", *Nature* **388**, 845-851 (1997).
3. G. F. Lipscomb, A. F. Garito, and R. S. Narang, "An exceptionally large linear electro-optic effect in the organic solid MNA," *J. Chem. Phys.* **75**, 1509-1516 (1981).
4. J. Xu, L. Zhou, and M. Thakur, "Measurement of electro-optic effects in single crystal films of N-(4-nitrophenyl)-L-prolinol," *Appl. Phys. Lett.* **69**, 1197-1198 (1996).
5. F. Pan, G. Knopfle, Ch. Bosshard, S. Follonier, R. Spreiter, M. S. Wong, and P. Gunter, "Electro-optic properties of the organic salt 4-N, N-dimethylamino-4'-N'-methyl-stilbazolium tosylate," *Appl. Phys. Lett.* **69**, 13-15 (1996).
6. L. R. Dalton, " Polymer electro-optic materials: optimization of electro-optic activity, minimization of optical loss, and fine-tuning of device performance", *Opt. Eng.* **39**(3), 589-595 (2000).
7. M. C. Oh, H. Zhang, C. Zhang, H. Erlig, Y. Chang, B. Tsap, D. Chang, A. Szep, W. H. Steier, H. R. Fetterman, and L. R. Dalton, " Recent advances in electrooptic polymer modulators incorporating highly nonlinear chromophore", *IEEE J. on Selected Topics in Quantum Electronics*, 7(5), 826-835 (2001).
8. D. Chen, H. R. Fetterman, A. Chen, W. H. Steier, L. R. Dalton, W. Wang, and Y. Shi, "Demonstration of 110 GHz electro-optic polymer modulators", *Appl. Phys. Lett.* **70**(25), 3335-3337 (1997).
9. C. C. Teng, and H. T. Man, "Simple Reflection Technique for Measuring the Electro-optic Coefficient of Poled Polymers", *Appl. Phys. Lett.* **56**(18), 1734-1736 (1990).
10. J. S. Schildkraut, "Determination of the Electrooptic Coefficient of a Poled Polymer Film", *Appl. Opt.* **29**(19), 2839-2841 (1990).
11. A. Chen, V. Chuyanov, H. Zhang, S. Garner, S. Lee, W. H. Steier, J. Chen, F. Wang, J. Zhu, M. He, Y. Ra, S. S. H. Mao, A. W. Harper, L. R. Dalton, and H. R. Fetterman, "DC Biased Electro-optic Polymer Waveguide Modulators with Low Half-wave Voltage and High Thermal Stability", *Opt. Eng.* **38**(12), 2000-2008 (1999).
12. S. S. Johal, S. W. James, R. P. Tatam, and G. J. Ashwell, "Second-harmonic Generation in Langmuir-Blodgett Waveguide Overlays on Single-mode Optical Fiber", *Opt. Lett.* **24**(17), 1194-1196 (1999).
13. S. Tang, Z. Shi, D. An, L. Sun, and R. T. Chen, "Highly Efficient Linear Waveguide Modulator Based on Domain-inverted Electro-optic Polymers", *Opt. Eng.* **39**, 680-688 (2000).
14. S. Yitzchaik, and T. J. Marks, "Chromophoric self-assembled superlattices", *Acc. Chem. Res.* **29**, 197-202 (1996).
15. Y. G. Zhao, A. Wu, H.-L. Lu, S. Chang, W.-K. Lu, and S. T. Ho, "Traveling wave electro-optic phase modulators based on intrinsically polar self-assembled chromophoric superlattices", *Appl. Phys. Lett.*, **79**(5), 587-589 (2001).